

# ENVIRONMENTAL RESEARCH

## CLIMATE



### OPEN ACCESS

RECEIVED  
1 May 2023

REVISED  
20 June 2023

ACCEPTED FOR PUBLICATION  
28 June 2023

PUBLISHED  
11 July 2023

### PAPER

## Contributions to regional precipitation change and its polar-amplified pattern under warming

David B Bonan<sup>1,\*</sup> , Nicole Feldl<sup>2</sup> , Mark D Zelinka<sup>3</sup> and Lily C Hahn<sup>4</sup>

<sup>1</sup> Environmental Science and Engineering, California Institute of Technology, Pasadena, CA, United States of America

<sup>2</sup> Earth and Planetary Sciences, University of California Santa Cruz, Santa Cruz, CA, United States of America

<sup>3</sup> Lawrence Livermore National Laboratory, Livermore, CA, United States of America

<sup>4</sup> Department of Atmospheric Sciences, University of Washington, Seattle, WA, United States of America

\* Author to whom any correspondence should be addressed.

E-mail: [dbonan@caltech.edu](mailto:dbonan@caltech.edu)

Original Content from this work may be used under the terms of the Creative Commons Attribution 4.0 licence.

Any further distribution of this work must maintain attribution to the author(s) and the title of the work, journal citation and DOI.



**Keywords:** precipitation, climate change, feedbacks, energy transport, polar climate

Supplementary material for this article is available [online](#)

### Abstract

The polar regions are predicted to experience the largest relative change in precipitation in response to increased greenhouse-gas concentrations, where a substantial absolute increase in precipitation coincides with small precipitation rates in the present-day climate. The reasons for this amplification, however, are still debated. Here, we use an atmospheric energy budget to decompose regional precipitation change from climate models under greenhouse-gas forcing into contributions from atmospheric radiative feedbacks, dry-static energy flux divergence changes, and surface sensible heat flux changes. The polar-amplified relative precipitation change is shown to be a consequence of the Planck feedback, which, when combined with larger polar warming, favors substantial atmospheric radiative cooling that balances increases in latent heat release from precipitation. Changes in the dry-static energy flux divergence contribute modestly to the polar-amplified pattern. Additional contributions to the polar-amplified response come, in the Arctic, from the cloud feedback and, in the Antarctic, from both the cloud and water vapor feedbacks. The primary contributor to the intermodel spread in the relative precipitation change in the polar region is also the Planck feedback, with the lapse rate feedback and dry-static energy flux divergence changes playing secondary roles. For all regions, there are strong covariances between radiative feedbacks and changes in the dry-static energy flux divergence that impact the intermodel spread. These results imply that constraining regional precipitation change, particularly in the polar regions, will require constraining not only individual feedbacks but also the covariances between radiative feedbacks and atmospheric energy transport.

### 1. Introduction

The polar regions are predicted to warm more than other regions in response to rising greenhouse-gas concentrations. This feature of climate change, referred to as 'polar amplification', has been a robust projection for several decades (Manabe and Wetherald 1975, Manabe and Stouffer 1980, Holland and Bitz 2003) and has been attributed to numerous processes such as sea ice changes (Manabe and Wetherald 1975, Holland and Bitz 2003, Winton 2006, Graversen and Wang 2009, Feldl and Merlis 2021), increased poleward energy transport (Holland and Bitz 2003, Hwang *et al* 2011, Singh *et al* 2017, Merlis and Henry 2018, Beer *et al* 2020), local radiative feedbacks (Pithan and Mauritsen 2014, Payne *et al* 2015, Stuecker *et al* 2018, Hahn *et al* 2021, Henry *et al* 2021), and interactions between poleward energy transport and radiative feedbacks (Bonan *et al* 2018, Russotto and Ackerman 2018, Feldl *et al* 2020, Previdi *et al* 2021, Beer and Eisenman 2022). However, despite the extensive amount of research on the polar amplification of temperature change, there are other aspects of the climate system that also exhibit polar-amplified changes in response to elevated

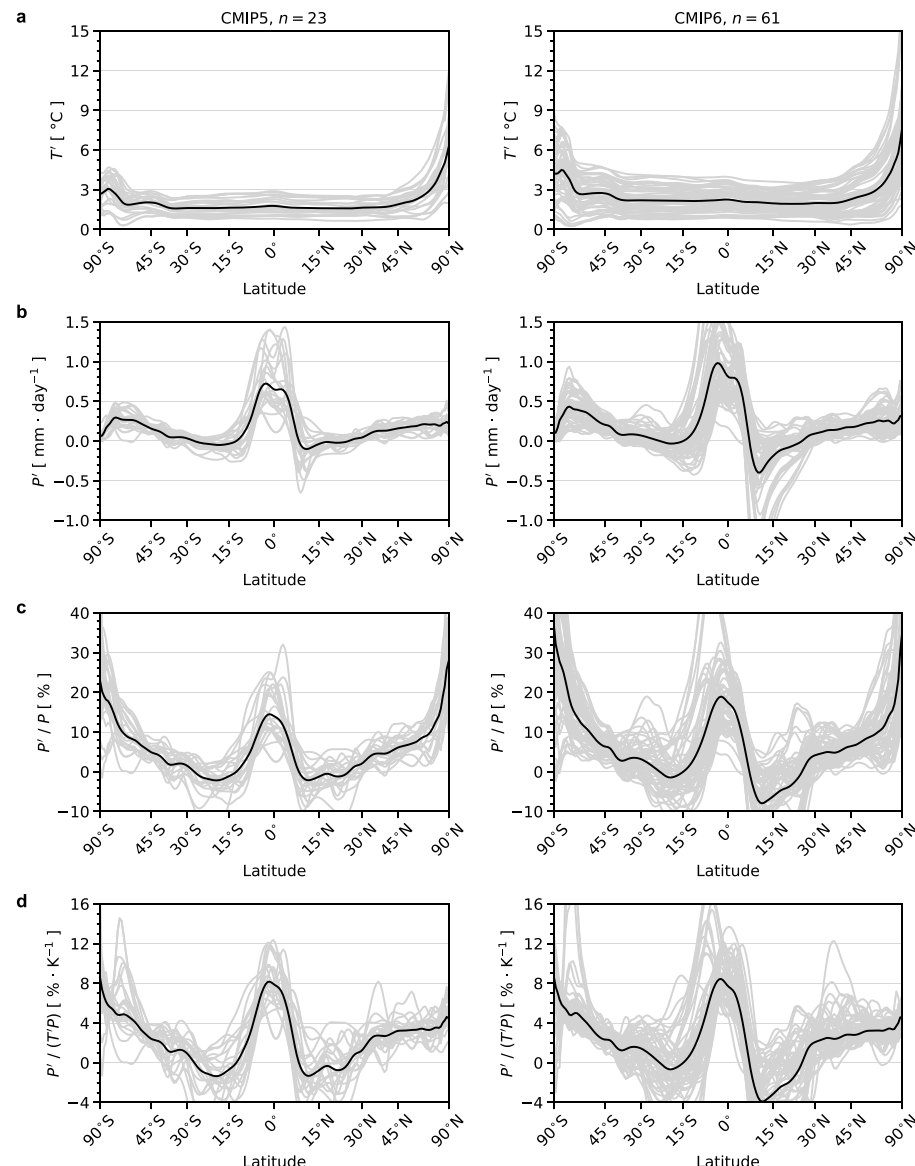


**Figure 1.** Patterns of temperature and precipitation change. The change in zonal-mean (a) near-surface air temperature, (b) precipitation, (c) precipitation normalized by the local precipitation climatology, and (d) precipitation normalized by the local precipitation climatology and local near-surface air temperature change. The black line denotes the multi-model mean and the grey lines denote individual GCMs. The left panel contains 23 GCM simulations from CMIP5 and the right panel contains 61 GCM simulations from CMIP6. Changes are computed as the difference between years 130–150 and years 1–20 in abrupt-4xCO<sub>2</sub> simulations.

greenhouse-gas concentrations. For example, under warming, the relative change in precipitation is also predicted to be largest in the polar regions, where a substantial absolute increase in precipitation coincides with small precipitation rates in the present-day climate (Bengtsson *et al* 2011, Bintanja and Selten 2014, Bintanja and Andry 2017, McCrystall *et al* 2021, Pithan and Jung 2021).

The larger relative precipitation change in the polar regions is a feature common to most comprehensive global climate models (GCMs) under greenhouse-gas forcing. Figure 1 shows the change in zonal-mean near-surface air temperature (figure 1(a)) and zonal-mean precipitation (figure 1(b)) for GCMs participating in phase 5 and phase 6 of the Coupled Model Intercomparison Project (CMIP5 and CMIP6) 130–150 years after an abrupt quadrupling of carbon-dioxide (abrupt-4xCO<sub>2</sub>) relative to years 1–20. The polar amplification of warming is larger in the Arctic than in the Antarctic, with the Arctic warming two-to-three times as much as other regions of the globe (figure 1(a)). This hemispheric asymmetry has been attributed to the lapse-rate feedback and Antarctic elevation (Salzmann 2017, Singh and Polvani 2020, Hahn *et al* 2021). Precipitation change occurs mainly in the tropics and extratropical high-latitudes (figure 1(b)), where GCMs predict an increase in precipitation between 0.5–1.5 mm · d<sup>-1</sup> in the tropics and 0.2–1.0 mm · d<sup>-1</sup> in the high-latitudes. However, the largest *relative* precipitation increase occurs both in

the Arctic and Antarctic (figure 1(c)), where small present-day precipitation rates coincide with a large increase in future precipitation. GCMs predict a relative increase in precipitation of 20%–40% in each polar region compared to 5%–20% in the tropics. Note, the relative precipitation change is slightly higher across most latitudes in CMIP6 (figure 1(c), right) when compared to CMIP5 (figure 1(c), left), which is likely related to overall higher transient warming and climate sensitivities in CMIP6 (Meehl *et al* 2020, Zelinka *et al* 2020). Even when the relative zonal-mean precipitation change is normalized by the local near-surface air temperature change (figure 1(d)), the Arctic and Antarctic still stand out as having much stronger hydrological sensitivity rates than any other latitude outside the tropics.

The polar amplification of precipitation change has largely been attributed to an increase in poleward moisture transport (Bengtsson *et al* 2011) and surface evaporation related to sea ice retreat (Bintanja and Selten 2014, Kopec *et al* 2016). However, more recent work that examined GCMs without sea ice loss has challenged this perspective and instead argued that precipitation change in the Arctic is mainly related to local radiative cooling changes that balance latent heat release from precipitation (Pithan and Jung 2021). Yet the exact processes that cause changes in radiative cooling remains unclear, and how these processes influence model projections of precipitation change has not been examined in detail. Indeed, a large body of work has shown that global-mean precipitation change can be energetically-constrained by radiative processes (e.g. Allen and Ingram 2002, Previdi 2010, O’Gorman *et al* 2012, Pendergrass and Hartmann 2014, DeAngelis *et al* 2015). These studies have shown that temperature and water vapor feedbacks contribute most to global-mean precipitation change and that the intermodel spread in global-mean precipitation change can be attributed to differences in atmospheric radiative cooling. However, a similar framework has not been used to quantify the role of radiative feedbacks on *regional* precipitation change. While recent work has shown that regional precipitation change can be energetically constrained (e.g. Muller and O’Gorman 2011, Anderson *et al* 2018, Labonté and Merlis 2020, Pithan and Jung 2021), the relative role of changes in radiative cooling and poleward energy transport in contributing to model projections of regional precipitation change remains poorly quantified. Arguably, knowledge of the processes that cause regional rather than global precipitation change is of greater consequence for society as this may ultimately inform local policy, particularly for Arctic communities which will experience the largest relative change in precipitation.

The purpose of this paper is to identify mechanisms for regional precipitation change under warming, with a particular focus on the polar amplification of precipitation change (see figures 1(c) and (d)). To do this, we use output from CMIP5 and CMIP6 GCMs and an atmospheric energy budget framework first introduced by Muller and O’Gorman (2011). In what follows, we first detail the atmospheric energy budget framework and describe the CMIP output. We then decompose regional precipitation change into contributions from individual atmospheric radiative feedbacks, the dry-static energy flux divergence changes, and the surface sensible heat flux changes. Finally, we use this framework to identify sources of intermodel spread in regional precipitation change under warming.

## 2. Data and methods

### 2.1. Atmospheric energy budget

To identify mechanisms for regional precipitation change  $P'$  we begin with a standard atmospheric energy budget. We define  $R'$  as the change in net top-of-atmosphere minus surface shortwave and longwave radiation;  $\nabla \cdot F'$  as the change in the atmospheric energy flux divergence,  $Q'_{\text{sensible}}$  as the change in the upward surface sensible heat flux, and  $Q'_{\text{latent}}$  as the change in the upward surface latent heat flux. All quantities are defined as annual mean so atmospheric energy and moisture storage can be neglected. Conservation of energy connects these variables via the following expression:

$$\nabla \cdot F' = R' + Q'_{\text{sensible}} + Q'_{\text{latent}}. \quad (1)$$

As noted by Muller and O’Gorman (2011) and Anderson *et al* (2018) because  $\nabla \cdot F'$  is comprised of both a dry-static  $\nabla \cdot F'_{\text{dry}}$  and a latent  $\nabla \cdot F'_{\text{latent}}$  component, and on annual-mean timescales  $\nabla \cdot F'_{\text{latent}}$  is equal to  $E' - P'$ , we can instead rewrite equation (1) as:

$$P' = -R' + \nabla \cdot F'_{\text{dry}} - Q'_{\text{sensible}}, \quad (2)$$

where the change in surface evaporation  $E'$  is cancelled out by the change in the upward surface latent heat flux (see Anderson *et al* (2018) for more details). Note,  $P'$  is in units of  $\text{W m}^{-2}$ , so it includes the latent heat of condensation (assumed constant and neglecting the latent heat of fusion for simplicity). We further partition  $R'$  into local atmospheric feedbacks,  $\lambda_{\text{atm}}$ , which are defined as difference between the top-of-atmosphere and surface radiative response per degree of zonal-mean near-surface air temperature change ( $\lambda_{\text{atm}} \equiv \lambda_{\text{toa}} - \lambda_{\text{sfc}}$ ). In this paper, we focus on changes between years 130–150 and years 1–20 in

abrupt-4xCO<sub>2</sub> simulations, which means radiative forcing is negligible (see below for more details). Thus equation (2) becomes:

$$P' = -\lambda_{\text{atm}} T' + \nabla \cdot F'_{\text{dry}} - Q'_{\text{sensible}} - \varepsilon, \quad (3)$$

where  $\varepsilon$  is a residual term and  $T'$  is the change in near-surface air temperature. Equation (3) relates regional precipitation change  $P'$  to four terms: atmospheric radiative feedbacks, changes in the dry-static energy flux divergence, changes in the upward surface sensible heat flux, and a residual term (which is small). Each term in equation (3) relates to local precipitation change through cooling or warming tendencies. Changes in the dry-static energy flux divergence, for instance, can lead to a cooling tendency through the export of heat which must be balanced by the latent heat release from precipitation and thus an increase in precipitation. However, it is important to note that each term is actually a response that corresponds to or balances the local precipitation change, and is therefore likely a combination of both cause and effect of the regional precipitation change. The net atmospheric radiative feedback  $\lambda_{\text{atm}}$  can be further decomposed into individual atmospheric radiative feedbacks (e.g. the surface albedo feedback, the lapse rate feedback, cloud feedbacks, etc). Equation (3) is similar to the expressions used by Muller and O'Gorman (2011) and Anderson *et al* (2018), except now the radiative cooling terms are accounted for through individual atmospheric radiative feedbacks representing distinct physical processes.

## 2.2. CMIP5 and CMIP6 output

To compute each term in equation (3) we use monthly mean output from abrupt-4xCO<sub>2</sub> simulations conducted by a suite of GCMs participating in CMIP5 and CMIP6 (see table S1 and S2 for more information). The change in each variable is computed as the difference in a climatology derived from years 130–150 of the simulation and a climatology derived from years 1–20 of the simulation. This is analogous to but simpler than computing the responses via linear regression over the 150 year simulation (Gregory *et al* 2004, Hansen *et al* 2005, Smith *et al* 2020). Because the carbon-dioxide concentration is held constant throughout the abrupt-4xCO<sub>2</sub> simulation, such epoch differences isolate the climate response that is mediated by increasing surface temperature, and avoids the need to account for the impact of radiative forcing or rapid adjustments to the radiative forcing.

The radiative feedbacks for each GCM are calculated using radiative kernels that quantify the sensitivity of top-of-atmosphere and surface downwelling radiation to small perturbations in surface and atmospheric temperature, water vapor, and surface albedo (Shell *et al* 2008, Soden *et al* 2008). We use recently developed ERA5-based top-of-atmosphere and surface radiative kernels (see Huang and Huang (2023) for more details). Each feedback is found by multiplying the relevant climate variable anomaly by the respective top-of-atmosphere and surface radiative kernel. For feedbacks due to atmospheric temperature and water vapor, the radiative response is vertically integrated up to the tropopause and then annually averaged. The total temperature feedback is further separated into the Planck and lapse rate components. The Planck feedback is the radiative flux anomaly associated with vertically uniform temperature change, and the lapse rate feedback is the radiative flux anomaly associated with changes in the vertical structure of temperature. Cloud feedbacks are computed by adjusting the change in cloud radiative effect for cloud masking effects, the latter computed by differencing clear- and all-sky non-cloud feedbacks (Soden *et al* 2008). The atmospheric radiative feedbacks are found by taking the difference between the top-of-atmosphere and surface radiative feedbacks (as noted in section 2.1). The multi-model and zonal-mean profiles of each local atmospheric radiative feedback are shown in figure S1. Top-of-atmosphere radiative feedbacks computed in this study show excellent agreement with top-of-atmosphere radiative feedbacks computed in previous studies that used a different set of radiative kernels and the Gregory regression method (e.g. Zelinka *et al* 2020, Zelinka 2022), giving us confidence in the accuracy of the radiative feedbacks derived here.

Finally, we compute the change in the surface sensible heat flux, near-surface air temperature, and dry-static energy flux divergence. The change in the dry-static energy flux divergence is computed from the difference in the change in net energy input into the atmosphere (top-of-atmosphere minus surface heat fluxes) and the change in latent energy flux divergence which is equal to the  $E' - P'$  (in W m<sup>-2</sup>).

## 3. Contributions to regional precipitation change

We begin by assessing the contribution of each mechanism in equation (3) to the zonal-mean structure of relative precipitation change for GCMs in CMIP5 and CMIP6, as outlined in section 2.1. The multi-model and zonal-mean precipitation change for years 130–150 (relative to years 1–20) is shown in figure 2. GCMs participating in both CMIP5 and CMIP6 show polar-amplified relative precipitation change, predicting a relative increase of 20%–40% in each polar region compared to an increase of 5%–20% in the tropics. GCMs

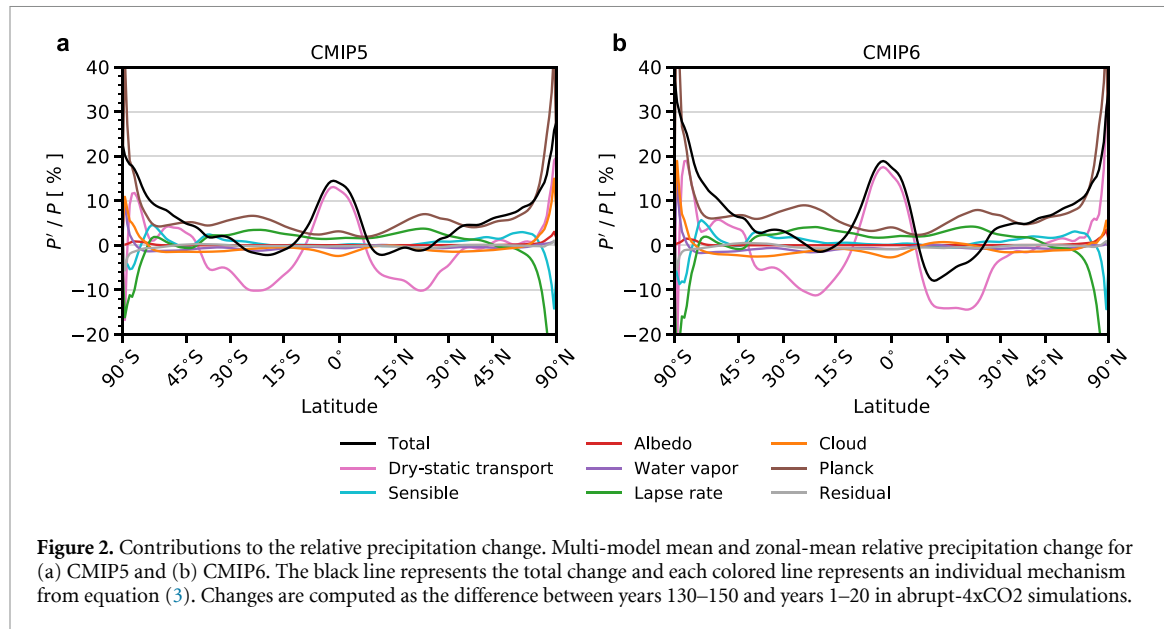


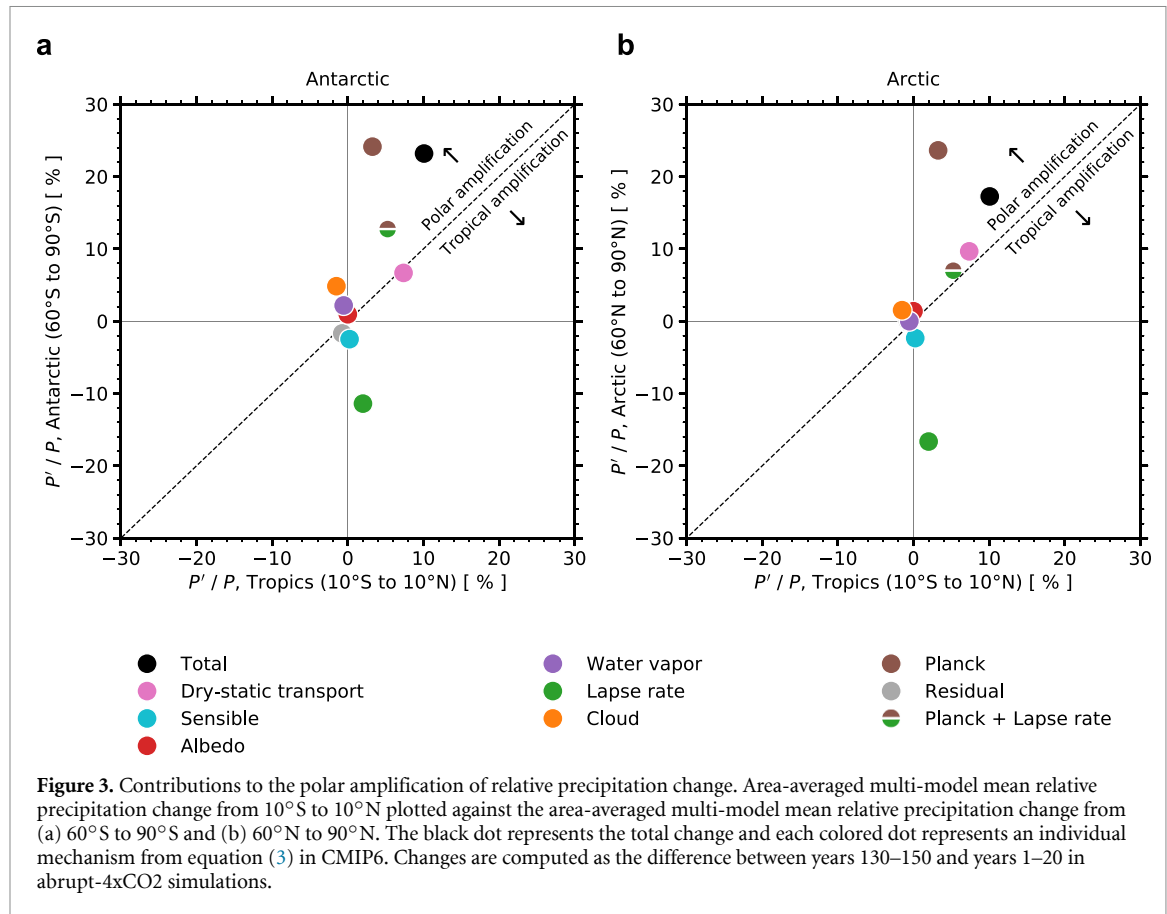
**Figure 2.** Contributions to the relative precipitation change. Multi-model mean and zonal-mean relative precipitation change for (a) CMIP5 and (b) CMIP6. The black line represents the total change and each colored line represents an individual mechanism from equation (3). Changes are computed as the difference between years 130–150 and years 1–20 in abrupt-4xCO<sub>2</sub> simulations.

in CMIP6 show an overall larger increase in precipitation when compared to CMIP5, and there is also a stronger decrease in Northern Hemisphere subtropical precipitation in CMIP6 when compared to CMIP5 (figures 2(a) and (b)). This is likely related to the overall higher transient warming and climate sensitivities of GCMs in CMIP6 (Meehl *et al* 2020, Zelinka *et al* 2020).

All mechanisms contribute to the zonal-mean structure of relative precipitation change, but the influence of each term is regionally distinct (figure 2). In the tropics (10°S to 10°N), an increase in the dry-static flux divergence contributes to almost all of the relative precipitation increase for both CMIP5 and CMIP6 (figures 2(a) and (b)). Greater export of dry-static energy in the tropics results in more atmospheric cooling which must be balanced by more latent heat release from precipitation. The cloud feedback (mainly the longwave component; not shown) contributes to a slight precipitation decrease in the deep tropics for both CMIP5 and CMIP6 (figures 2(a) and (b)). In the subtropics (10°S/N to 30°S/N), an increase in the dry-static energy flux convergence contributes to the slight decrease in precipitation; the greater drying of the Northern Hemisphere subtropics, particularly in CMIP6, arises from hemispheric asymmetries in the dry-static energy flux divergence and likely hemispheric asymmetries in Hadley circulation changes. The subtropical increase in the dry-static energy flux convergence is also largely opposed by the lapse rate and Planck feedbacks (figure 2). For CMIP5 and CMIP6, both the lapse rate and Planck feedback contribute to radiative cooling in the tropics and subtropics, which is balanced by an increase in precipitation and latent heat release (figure 2).

In the polar regions, a number of processes contribute to the relative precipitation change. Reduced dry-static energy flux convergence contributes to an overall increase in precipitation in both polar regions. A reduction in the meridional temperature gradient in both hemispheres reduces the dry-static flux convergence in the polar regions and therefore contributes to a cooling tendency that is balanced by an increase in precipitation due to latent heat release. The contribution of dry-static energy flux convergence changes in the Arctic is slightly higher in CMIP6 than in CMIP5, likely because CMIP6 GCMs exhibit stronger Arctic amplification (Hahn *et al* 2021), which results in a greater reduction in the dry-static energy flux convergence and thus more of a cooling tendency. The Planck feedback contributes even more to the overall increase in precipitation in the polar regions, where combined with polar-amplified warming, there is substantial local radiative cooling. The Planck feedback contributes to 40%–60% of the relative precipitation increase in both polar regions, with changes in the dry-static flux divergence contributing to 10%–30%.

Most other terms contribute to decreases in precipitation or small increases in precipitation. Surface sensible heat flux changes contribute slightly to the relative precipitation increase, particularly in subpolar regions where ocean circulations shape the degree of surface warming (Marshall *et al* 2015). At higher-latitudes, the surface sensible heat flux changes contribute to a decrease in precipitation. In both polar regions, the net cloud feedback (including shortwave and longwave processes; not shown) contributes some to the relative increase in precipitation. The lapse rate feedback, which is strongly positive in the polar regions, contributes to a large decrease in precipitation in both polar regions. Notably, the decrease in precipitation associated with the lapse rate feedback is much smaller in the Antarctic when compared to the Arctic, despite the Planck feedback contributing to a similar precipitation increase in both regions. This is



likely related to the fact that the lapse rate feedback is strongly influenced by Antarctic ice-sheet elevation (Hahn *et al* 2020). Finally, in contrast to studies examining polar warming using a top-of-atmosphere perspective (e.g. Pithan and Mauritsen 2014, Hahn *et al* 2021), the surface-albedo feedback contributes only slightly to the increase in precipitation in both polar regions for both CMIP5 and CMIP6 (figure 2). However, this reflects the fact that most surface-albedo changes are radiated directly to space, not absorbed in the atmosphere. The water vapor feedback is similarly a small contributor, with the exception of the Antarctic, where the feedback is negative (figure S1) and the associated precipitation change, positive.

### 3.1. Polar amplification of precipitation change

We next examine contributions to the polar-amplified pattern of relative precipitation change in CMIP6 by following Pithan and Mauritsen (2014) and Hahn *et al* (2021), and plotting relative precipitation change on a scatter plot where the x-axis represents the area-weighted averaged of each term in the tropics and the y-axis represents the area-weighted averaged of each term in the polar regions. The polar regions are defined from  $60^{\circ}\text{S/N}$  to  $90^{\circ}\text{S/N}$ , while the tropical region is defined as  $10^{\circ}\text{S}$  to  $10^{\circ}\text{N}$ . This is slightly different from the tropical domain used by other studies that examine contributions to the polar amplification of warming, but because precipitation change exhibits a more narrowly peaked pattern in the tropics, we opt to define a smaller tropical domain. The following results are similar for a tropical region averaged from  $30^{\circ}\text{S}$  to  $30^{\circ}\text{N}$ , but the influence of changes in the dry-static energy flux divergence on tropical precipitation change decreases slightly (see figure S2). The results are also similar for CMIP5 (see figure S3). Changes that fall above the one-to-one line contribute to polar amplification of relative precipitation change whereas changes that fall below the one-to-one line contribute to tropical amplification of relative precipitation change.

The key contribution to the amplification of relative precipitation change in the polar regions is the Planck feedback, giving a factor of six increase in the Antarctic and Arctic relative to the tropics (figures 3(a) and (b)). Changes in the dry-static energy flux divergence contribute almost equally to the relative change in precipitation in both the Antarctic and Arctic when compared to the tropics. The lapse rate feedback contributes to a tropical-amplified precipitation response relative to both polar regions causing approximately a 2% increase in the tropics and a 10% and 20% decrease in the Antarctic and Arctic, respectively. However, the combined contribution of the total temperature feedback (Planck and lapse rate) results in a weaker polar-amplified response in both polar regions (figure 3, brown/green dot). In the Arctic,

the combined temperature feedback, cloud feedback, and the dry-static energy flux divergence contribute a similar amount to the polar-amplified response, while in the Antarctic, the combined temperature feedback contributes more to the polar-amplified response. The combined temperature feedback might also explain why the Antarctic has a larger local hydrological sensitivity than the Arctic (see figure 1(d)), as a weaker lapse rate feedback favors stronger net radiative cooling relative to the Arctic. In both the Antarctic and Arctic, the cloud feedback also contributes slightly to the polar-amplified precipitation response causing a 2% decrease in the tropics and a 6% and 2% increase in the Antarctic and Arctic, respectively. In the Antarctic, the water vapor feedback contributes slightly to the amplified precipitation response, while in the Arctic, the water vapor feedback does not contribute to the amplified precipitation response. In both polar regions, the surface-albedo feedback contributes little to the polar-amplified response (figure 3).

### 3.2. Sources of intermodel spread in regional precipitation change

We next investigate sources of intermodel spread in the relative change in precipitation for the tropics, subtropics, and polar regions by examining the contribution of each mechanism in equation (3) for each GCM from CMIP6. We focus on CMIP6, but similar results are obtained for the CMIP5 intermodel spread (see figure S4). In the Arctic (60 °N to 90 °N), the single largest contributor to the intermodel spread in relative precipitation change is the Planck feedback, where combined with large intermodel differences in Arctic warming, there is substantial intermodel spread in radiative cooling (figure 4(a)). Changes in the dry-static energy flux divergence also contribute to the intermodel spread (figure 4(a)). Notably, the lapse rate feedback and surface sensible heat flux changes contribute negatively to the intermodel spread, meaning GCMs with larger relative precipitation increases exhibit more negative contributions from these two terms (figure 4(a), left). The surface-albedo feedback contributes little to the intermodel spread (figure 4(a)).

In the Northern Hemisphere subtropics (10 °N to 30 °N), an increase in the dry-static energy flux convergence dominates the intermodel spread in relative precipitation change, with little contribution from atmospheric radiative feedbacks or surface sensible heat flux changes (figure 4(b)). Similarly, in the tropics (10 °S to 10 °N), most of the intermodel spread in regional relative precipitation change is attributed to a increase in the dry-static energy flux divergence (figure 4(c)). The other terms, including cloud feedbacks, contribute little to the intermodel spread. In fact, cloud feedbacks dampen the intermodel spread as GCMs with larger relative precipitation increases exhibit slightly more negative contributions from cloud feedbacks (figure 4(c)). A similar picture emerges for the Southern Hemisphere subtropics (10 °S to 30 °S); changes in the dry-static energy flux divergence dominates the intermodel spread in subtropical precipitation decrease (figure 4(d)). However, in contrast to the Northern Hemisphere subtropics, the Planck feedback also contributes some to the intermodel spread in the Southern Hemisphere subtropics (figures 4(b) and (d)).

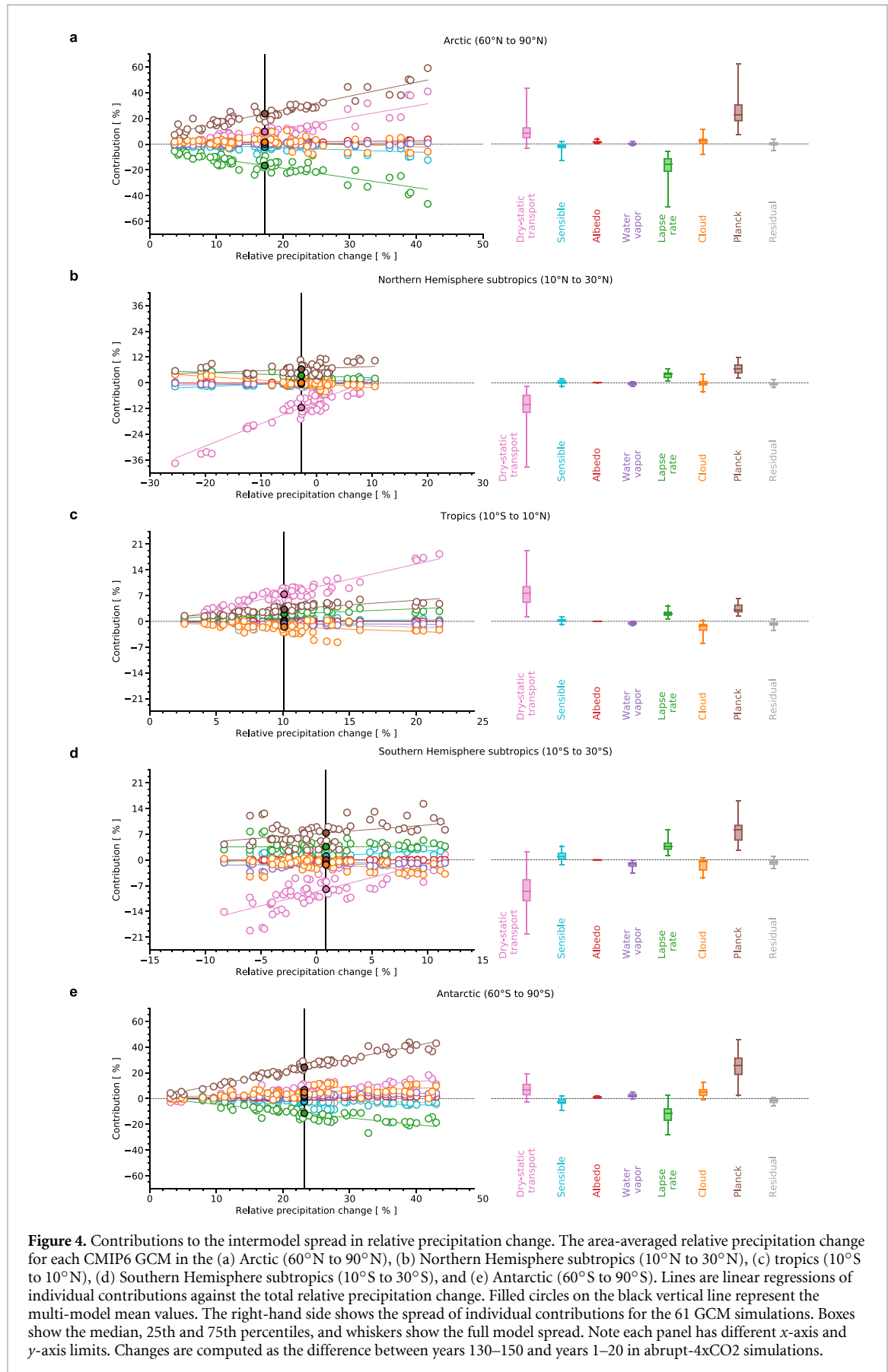
Finally, in the Antarctic (60 °S to 90 °S), the intermodel spread in relative precipitation change is also dominated by both the Planck feedback and changes in the dry-static energy flux divergence (figure 4(e)). The cloud feedback also contributes to the intermodel spread, however, it only contributes to approximately 20% of the total intermodel spread (figure 4(e)). As with the Arctic, the surface sensible heat flux and lapse rate feedback contributes negatively to the intermodel spread in the Antarctic, meaning GCMs with higher relative precipitation change exhibit more negative contributions from these two terms (figure 4(e), left).

Because the intermodel spread in regional precipitation change is impacted not only by the variance of each term but also by their covariances, we follow Caldwell *et al* (2016) and Hahn *et al* (2021) and compute a covariance matrix of equation (3). The variance budget for a linear combination of variables is:

$$\text{var} \left( \sum_{i=1}^N X_i \right) = \sum_{i=1}^N \text{var}(X_i) + 2 \sum_{j=1}^N \sum_{k=j+1}^N \text{cov}(X_j, X_k). \quad (4)$$

Here,  $X_i$  represents each mechanism in equation (3) from GCMs in CMIP6. Variances for each term appear on the main diagonal, while covariance terms are on the off diagonals. However, because the covariance matrix is symmetric, each covariance must be included twice. So we instead double the value of covariances above the main diagonal and omit the corresponding covariances below the diagonal. Covariance terms can be positive or negative while variances are always positive. To easily interpret the covariance matrix, we normalize the covariance matrix by the variance in relative precipitation change for each region such that the sum of each covariance matrix is one.

Figure 5 shows the covariance matrix of each mechanism in equation (3) from CMIP6 GCMs for the tropics, subtropics, and polar regions. Consistent with figure 4, the main diagonal for the Arctic shows large variances contributed by the Planck feedback, changes in the dry-static energy flux divergence, and the lapse rate feedback (figure 5(a)). Additionally, a strong positive covariance between the Planck feedback and changes in the dry-static energy flux divergence amplifies the intermodel spread. A positive covariance arises



because more Arctic warming implies stronger radiative cooling associated with the Planck feedback, but also less dry-static energy flux convergence due to a reduction in the meridional temperature gradient, both of which cause cooling and an increase in precipitation. Conversely, a negative covariance between dry-static

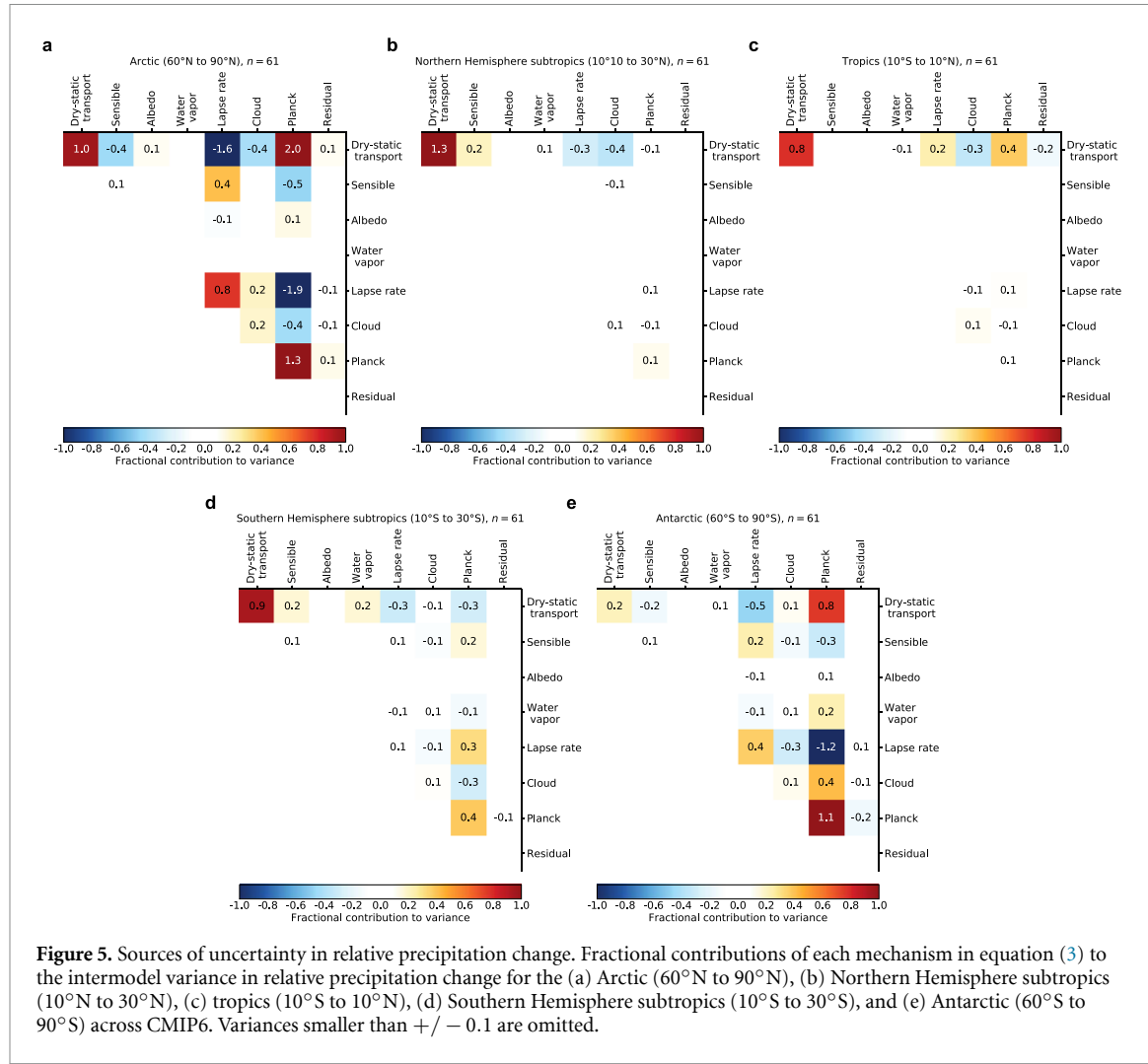


**Figure 5.** Sources of uncertainty in relative precipitation change. Fractional contributions of each mechanism in equation (3) to the intermodel variance in relative precipitation change for the (a) Arctic ( $60^{\circ}\text{N}$  to  $90^{\circ}\text{N}$ ), (b) Northern Hemisphere subtropics ( $10^{\circ}\text{N}$  to  $30^{\circ}\text{N}$ ), (c) tropics ( $10^{\circ}\text{S}$  to  $10^{\circ}\text{N}$ ), (d) Southern Hemisphere subtropics ( $10^{\circ}\text{S}$  to  $30^{\circ}\text{S}$ ), and (e) Antarctic ( $60^{\circ}\text{S}$  to  $90^{\circ}\text{S}$ ) across CMIP6. Variances smaller than  $\pm 0.1$  are omitted.

energy flux divergence changes and the lapse rate feedback and the surface sensible heat flux changes slightly dampens the intermodel spread (figure 5(a)). Negative covariances arise because the lapse rate feedback and surface sensible heat flux changes contribute to Arctic warming which causes a precipitation decrease, but Arctic warming also reduces the meridional temperature gradient and therefore reduces the dry-static energy flux convergence in the polar regions, contributing to slight cooling and thus an increase in precipitation. A strong negative covariance between the Planck and lapse-rate feedback in the Arctic strongly dampens the intermodel spread (figure 5(a)). A negative covariance here arises because in the Arctic, and polar regions more broadly, warming results in more radiative cooling from the Planck feedback but also more radiative warming from the lapse-rate feedback.

In the subtropics and tropics, the main contributor to the intermodel spread is changes in the dry-static energy flux divergence (figures 5(b)–(d)). However, there are small, but significant, negative covariances between the cloud feedback and dry-static energy flux divergence changes that slightly dampens the intermodel spread in the tropics and Northern Hemisphere subtropics (figures 5(b) and (c)). This is consistent with Schiro *et al* (2022) who found a strong connection between the low cloud feedback and the Hadley circulation, which are the dominant component of dry-static energy transport in the tropics and subtropics.

Finally, in the Antarctic, the dominant contributor to the intermodel spread in relative precipitation change is also the Planck feedback, but strong positive covariances exist for other terms that also play a leading role (figure 5(e)). For example, like in the Arctic, there is a strong positive covariance between the Planck feedback and changes in dry-static energy flux divergence that contributes substantially to the intermodel variance (figure 5(e)). There is also a strong negative covariance between the lapse rate feedback and changes in dry-static energy flux divergence that contributes negatively to intermodel spread (figure 5(e)).

#### 4. Discussion and conclusions

In response to increased greenhouse-gas concentrations, comprehensive GCMs predict that precipitation will increase mostly in the tropics and high-latitudes. However, the *relative* change in precipitation is predicted to be largest in the polar regions, where a substantial absolute increase in precipitation coincides with small precipitation rates in the present-day climate (figures 1(c) and (d)). Understanding the causes of regional precipitation change and the higher rates of relative precipitation change in the polar regions remains an active area of research.

In this paper, we used an atmospheric energy budget to decompose regional precipitation change in abrupt-4xCO<sub>2</sub> simulations from GCMs in CMIP5 and CMIP6 into contributions from atmospheric radiative feedbacks, dry-static energy flux divergence changes, and surface sensible heat flux changes. In the tropics and subtropics, precipitation change is dominated by changes in the dry-static energy flux divergence—consistent with Muller and O’Gorman (2011). In the polar regions, changes in radiative cooling, rather than changes in the dry-static energy flux divergence, dominate precipitation change—which is also consistent with Pithan and Jung (2021). However, we further showed that the primary reason for the radiative cooling changes in both polar regions is the Planck feedback, which quantifies the radiative flux anomaly associated with vertically-uniform tropospheric warming equal to that of the surface, and is a robust feature of the climate response. The polar-amplified pattern of warming results in more radiative cooling associated with the Planck feedback, which is balanced by an increase in precipitation associated with latent heat release. This explains why the relatively large increase in precipitation in the polar regions is a common feature of GCMs, as GCMs share similar Planck feedbacks and patterns of polar-amplified warming (Tebaldi and Arblaster 2014). However, there is a strong compensation from the lapse rate feedback that acts to reduce the influence of the Planck feedback in the Arctic and Antarctic. Modest additional contributions to the polar-amplified response come, in the Arctic, from the cloud feedback and, in the Antarctic, from the cloud feedback and water vapor feedback.

We also used the atmospheric energy budget framework to examine the intermodel spread in regional precipitation change. In the polar regions, the intermodel spread in relative precipitation change is dominated by the Planck feedback and polar warming, with the lapse rate feedback and dry-static energy flux divergence changes playing secondary roles. In all regions, including the subtropics and tropics, large covariances exist between radiative feedbacks and changes in the dry-static energy flux divergence that act to amplify or dampen the intermodel spread. For example, in the tropics, cloud feedbacks and changes in the dry-static energy flux divergence have a fairly strong negative covariance that dampens the intermodel spread, while in the Arctic, the Planck feedback and dry-static energy flux divergence changes have a strong positive covariance that amplifies the intermodel spread.

Despite the utility of this framework for decomposing model projections of regional precipitation change into individual mechanisms, it is well understood that radiative feedbacks alter atmospheric energy transport (e.g. Hwang *et al* 2011, Zelinka and Hartmann 2012, Feldl *et al* 2017). A limitation of using a fixed atmospheric energy budget to diagnose mechanisms of regional precipitation change is that it implicitly includes interactions between radiative feedbacks, making mechanistic interpretation difficult. For example, the strength of the lapse-rate feedback may be impacted by the amount of surface warming contributed by the surface-albedo feedback (e.g. Graversen *et al* 2014, Feldl *et al* 2017, 2020). An alternative perspective may be provided by ‘feedback locking’ experiments similar to those of Beer and Eisenman (2022), where atmospheric energy transport and other feedbacks can interact with each other in an energy balance model of hydrological changes (e.g. Siler *et al* 2018, Bonan *et al* 2023). Indeed, some of these interactions and relationships are evident in the covariance analysis of section 3.2 (see figure 5). This analysis shows large covariances between radiative feedbacks and changes in the dry-static energy flux divergence in the polar regions. Similarly, in the tropics, the negative covariance between the cloud feedback and changes in the dry-static energy flux divergence indicates that the cloud feedback and dry-static energy transport, which is primarily accomplished by the Hadley circulation, are strongly related. Future work should explore how radiative feedbacks interact with dry-static energy transport to alter regional precipitation change.

Our study also contains a few other caveats. First, this framework is a purely diagnostic approach and does not allow for determination of causality. Each term in equation (3) is actually a response that corresponds to or balances the regional precipitation change, and is therefore a combination of cause and effect of regional precipitation change. Applying this framework to transient climate change experiments might improve mechanistic interpretations of regional precipitation change. Second, we only focused on annual changes. It is well known that some of the largest changes to precipitation are predicted to occur in winter, when the amplification of temperature change is also strongest (e.g. Pithan and Mauritsen 2014, Pithan and Jung 2021). Examining the seasonality of precipitation change through an atmospheric energy budget perspective may change the impact of each mechanism on regional precipitation change. Third, other

work has shown that precipitation exhibits a so-called 'fast' and 'slow' response to radiative forcing and temperature changes, respectively (Yang *et al* 2003, Andrews and Forster 2010, Bala *et al* 2010). We ignored the fast response of precipitation change, but the framework introduced in this paper could be used to understand differences in the fast and slow responses of regional precipitation to radiative forcing. Finally, we did not normalize the precipitation change from each GCM by the amount of warming, which might account for some of the intermodel spread in regional precipitation change.

Overall, we show the Arctic and Antarctic exhibit larger relative increases in precipitation under greenhouse-gas forcing because of the Planck feedback and polar amplification of warming, which favors strong radiative cooling that is balanced by an increase in latent heat release associated with precipitation. This explains why most GCMs exhibit a polar-amplified precipitation response, as both the Planck feedback and polar-amplified warming are fundamental aspects of the climate response to greenhouse-gas forcing. Much of the intermodel spread in polar precipitation change can be also be attributed to the Planck feedback. However, other components and their covariances can contribute substantially to the intermodel spread in regional precipitation change. For example, in the polar regions, a covariance between the Planck feedback and changes in the dry-static energy flux divergence also contribute to the intermodel spread because more polar warming leads to stronger radiative cooling from the Planck feedback but also a reduction in the meridional temperature gradient that reduces poleward dry-static energy transport. Both of these processes result in a cooling tendency that is balanced by latent heat release from an increase in precipitation. A key implication of this work is that constraining regional precipitation change will require constraining not only individual radiative feedbacks, but also the covariances between them, which can contribute equally if not more to the intermodel spread in regional precipitation change. More broadly this work highlights the need to better understand interactions between radiative feedbacks and poleward energy transport, and their connection to regional hydrological changes.

## Data availability statement

All data that support the findings of this study are included within the article (and any supplementary information files) and can be found at the Earth System Grid Federation (ESGF) Portal (<https://esgf-node.llnl.gov/search/cmip5/> and <https://esgf-node.llnl.gov/search/cmip6/>).

## Acknowledgment

The authors thank the climate modeling groups for producing and making available their output. The authors also thank Yi Huang and Han Huang for providing the ERA5-based surface and top-of-atmosphere radiative kernels. The authors are grateful for two reviewers and the editor for helpful and encouraging comments. D B B was supported by the National Science Foundation (NSF) Graduate Research Fellowship Program (NSF Grant DGE-1745301). N F was supported by NSF Award AGS-1753034. M D Z was supported by the U.S. Department of Energy (DOE) Regional and Global Model Analysis program area and his work was performed under the auspices of the U.S. DOE by Lawrence Livermore National Laboratory under Contract DE-AC52-07NA27344. L C H was supported by the NSF Graduate Research Fellowship Program (NSF Grant DGE-1762114).

## ORCID iDs

David B Bonan  <https://orcid.org/0000-0003-3867-6009>  
Nicole Feldl  <https://orcid.org/0000-0002-2631-1419>  
Mark D Zelinka  <https://orcid.org/0000-0002-6570-5445>  
Lily C Hahn  <https://orcid.org/0000-0002-0573-5183>

## References

Allen M R and Ingram W J 2002 Constraints on future changes in climate and the hydrologic cycle *Nature* **419** 228–32  
Anderson B T, Feldl N and Lintner B R 2018 Emergent behavior of Arctic precipitation in response to enhanced Arctic warming *J. Geophys. Res. Atmos.* **123** 2704–17  
Andrews T and Forster P M 2010 The transient response of global-mean precipitation to increasing carbon dioxide levels *Environ. Res. Lett.* **5** 025212  
Bala G, Caldeira K and Nemani R 2010 Fast versus slow response in climate change: implications for the global hydrological cycle *Clim. Dyn.* **35** 423–34  
Beer E and Eisenman I 2022 Revisiting the role of the water vapor and lapse rate feedbacks in the Arctic amplification of climate change *J. Clim.* **35** 2975–88  
Beer E, Eisenman I and Wagner T J 2020 Polar amplification due to enhanced heat flux across the halocline *Geophys. Res. Lett.* **47** e2019GL086706

Bengtsson L, Hodges K I, Koumoutsaris S, Zahn M and Keenlyside N 2011 The changing atmospheric water cycle in Polar Regions in a warmer climate *Tellus A* **63** 907–20

Bintanja R and Andry O 2017 Towards a rain-dominated Arctic *Nat. Clim. Change* **7** 263–7

Bintanja R and Selten F 2014 Future increases in Arctic precipitation linked to local evaporation and sea-ice retreat *Nature* **509** 479–82

Bonan D B, Siler N, Roe G H and Armour K C 2023 Energetic constraints on the pattern of changes to the hydrological cycle under global warming *J. Clim.* **46** 3499–522

Bonan D, Armour K, Roe G, Siler N and Feldl N 2018 Sources of uncertainty in the meridional pattern of climate change *Geophys. Res. Lett.* **45** 9131–40

Caldwell P M, Zelinka M D, Taylor K E and Marvel K 2016 Quantifying the sources of intermodel spread in equilibrium climate sensitivity *J. Clim.* **29** 513–24

DeAngelis A M, Qu X, Zelinka M D and Hall A 2015 An observational radiative constraint on hydrologic cycle intensification *Nature* **528** 249–53

Feldl N, Bordoni S and Merlis T M 2017 Coupled high-latitude climate feedbacks and their impact on atmospheric heat transport *J. Clim.* **30** 189–201

Feldl N and Merlis T M 2021 Polar amplification in idealized climates: the role of ice, moisture and seasons *Geophys. Res. Lett.* **48** e2021GL094130

Feldl N, Po-Chedley S, Singh H K, Hay S and Kushner P J 2020 Sea ice and atmospheric circulation shape the high-latitude lapse rate feedback *njp clim. Atmos. Sci.* **3** 1–9

Graversen R G, Langen P L and Mauritsen T 2014 Polar amplification in CCSM4: contributions from the lapse rate and surface albedo feedbacks *J. Clim.* **27** 4433–50

Graversen R G and Wang M 2009 Polar amplification in a coupled climate model with locked albedo *Clim. Dyn.* **33** 629–43

Gregory J, Ingram W, Palmer M, Jones G, Stott P, Thorpe R, Lowe J, Johns T and Williams K 2004 A new method for diagnosing radiative forcing and climate sensitivity *Geophys. Res. Lett.* **31** L03205

Hahn L C, Armour K C, Battisti D S, Donohoe A, Pauling A and Bitz C M 2020 Antarctic elevation drives hemispheric asymmetry in polar lapse rate climatology and feedback *Geophys. Res. Lett.* **47** e2020GL088965

Hahn L C, Armour K C, Zelinka M D, Bitz C M and Donohoe A 2021 Contributions to polar amplification in CMIP5 and CMIP6 models *Front. Earth Sci.* **9** 710036

Hansen J *et al* 2005 Efficacy of climate forcings *J. Geophys. Res. Atmos.* **110** D18104

Henry M, Merlis T M, Lutsko N J and Rose B E 2021 Decomposing the drivers of polar amplification with a single-column model *J. Clim.* **34** 2355–65

Holland M M and Bitz C M 2003 Polar amplification of climate change in coupled models *Clim. Dyn.* **21** 221–232

Huang H and Huang Y 2023 Radiative sensitivity quantified by a new set of radiation flux kernels based on the ERA5 reanalysis *Earth Syst. Sci. Data Discuss.* 1–36

Hwang Y-T, Frierson D M and Kay J E 2011 Coupling between Arctic feedbacks and changes in poleward energy transport *Geophys. Res. Lett.* **38** 38

Kopecky B G, Feng X, Michel F A and Posmentier E S 2016 Influence of sea ice on Arctic precipitation *Proc. Natl Acad. Sci.* **113** 46–51

Labonté M-P and Merlis T M 2020 Sensitivity of the atmospheric water cycle within the habitable zone of a tidally locked, Earth-like exoplanet *Astrophys. J.* **896** 31

Manabe S and Stouffer R J 1980 Sensitivity of a global climate model to an increase of CO<sub>2</sub> concentration in the atmosphere *J. Geophys. Res.* **85** 5529–54

Manabe S and Wetherald R T 1975 The effects of doubling the CO<sub>2</sub> concentration on the climate of a general circulation model *J. Atmos. Sci.* **32** 3–15

Marshall J, Scott J R, Armour K C, Campin J-M, Kelley M and Romanou A 2015 The ocean's role in the transient response of climate to abrupt greenhouse gas forcing *Clim. Dyn.* **44** 2287–99

McCrystall M R, Stroeve J, Serreze M, Forbes B C and Screen J A 2021 New climate models reveal faster and larger increases in Arctic precipitation than previously projected *Nat. Commun.* **12** 6765

Meehl G A, Senior C A, Eyring V, Flato G, Lamarque J-F, Stouffer R J, Taylor K E and Schlund M 2020 Context for interpreting equilibrium climate sensitivity and transient climate response from the CMIP6 Earth system models *Sci. Adv.* **6** eaba1981

Merlis T M and Henry M 2018 Simple estimates of polar amplification in moist diffusive energy balance models *J. Clim.* **31** 5811–24

Muller C J and O'Gorman P 2011 An energetic perspective on the regional response of precipitation to climate change *Nat. Clim. Change* **1** 266–71

O'Gorman P A, Allan R P, Byrne M P and Previdi M 2012 Energetic constraints on precipitation under climate change *Surv. Geophys.* **33** 585–608

Payne A E, Jansen M F and Cronin T W 2015 Conceptual model analysis of the influence of temperature feedbacks on polar amplification *Geophys. Res. Lett.* **42** 9561–70

Pendergrass A G and Hartmann D L 2014 The atmospheric energy constraint on global-mean precipitation change *J. Clim.* **27** 757–68

Pithan F and Jung T 2021 Arctic amplification of precipitation changes—the energy hypothesis *Geophys. Res. Lett.* **48** e2021GL094977

Pithan F and Mauritsen T 2014 Arctic amplification dominated by temperature feedbacks in contemporary climate models *Nat. Geosci.* **7** 181–4

Previdi M 2010 Radiative feedbacks on global precipitation *Environ. Res. Lett.* **5** 025211

Previdi M, Smith K L and Polvani L M 2021 Arctic amplification of climate change: a review of underlying mechanisms *Environ. Res. Lett.* **16** 093003

Russotto R D and Ackerman T P 2018 Energy transport, polar amplification and ITCZ shifts in the GeoMIP G1 ensemble *Atmos. Chem. Phys.* **18** 2287–305

Salzmann M 2017 The polar amplification asymmetry: role of Antarctic surface height *Earth Syst. Dyn.* **8** 323–36

Schiavo K A *et al* 2022 Model spread in tropical low cloud feedback tied to overturning circulation response to warming *Nat. Commun.* **13** 7119

Shell K M, Kiehl J T and Shields C A 2008 Using the radiative kernel technique to calculate climate feedbacks in NCAR's Community Atmospheric Model *J. Clim.* **21** 2269–82

Siler N, Roe G H and Armour K C 2018 Insights into the zonal-mean response of the hydrologic cycle to global warming from a diffusive energy balance model *J. Clim.* **31** 7481–93

Singh H A and Polvani L M 2020 Low Antarctic continental climate sensitivity due to high ice sheet orography *njp Clim. Atmos. Sci.* **3** 1–10

Singh H, Rasch P and Rose B 2017 Increased ocean heat convergence into the high latitudes with CO<sub>2</sub> doubling enhances polar-amplified warming *Geophys. Res. Lett.* **44** 10–583

Smith C J *et al* 2020 Effective radiative forcing and adjustments in CMIP6 models *Atmos. Chem. Phys.* **20** 9591–618

Soden B J, Held I M, Colman R, Shell K M, Kiehl J T and Shields C A 2008 Quantifying climate feedbacks using radiative kernels *J. Clim.* **21** 3504–20

Stuecker M F *et al* 2018 Polar amplification dominated by local forcing and feedbacks *Nat. Clim. Change* **8** 1076–81

Tebaldi C and Arblaster J M 2014 Pattern scaling: its strengths and limitations and an update on the latest model simulations *Clim. Change* **122** 459–71

Winton M 2006 Amplified Arctic climate change: what does surface albedo feedback have to do with it? *Geophys. Res. Lett.* **33** L03701

Yang F, Kumar A, Schlesinger M E and Wang W 2003 Intensity of hydrological cycles in warmer climates *J. Clim.* **16** 2419–23

Zelinka M D 2020 Causes of higher climate sensitivity in CMIP6 models *Geophys. Res. Lett.* **47** e2019GL085782

Zelinka M D 2022 CMIP5/6 Forcing, Feedbacks, and ECS Zenodo <https://doi.org/10.5281/zenodo.6647291>

Zelinka M D and Hartmann D L 2012 Climate feedbacks and their implications for poleward energy flux changes in a warming climate *J. Clim.* **25** 608–24